Vol. 7, No. 3, November 2025 (Special Issue), pp. 321~336, p-ISSN 2685-2381, e-ISSN 2715-2626
http://dx.doi.org/10.28989/avitec.v7i3.3119

Optimization of BLDC Motor Geometry using Particle Swarm Optimization Algorithm to Achieve Efficiency Balance Across Various Electric Vehicle Traction Requirements

Kurniawan*, Hasanudin, Agus Dwiyanto, Rivanda Tyaksa Putra
Department of Electrical Engineering, Institut Teknologi Nasional Yogyakarta, Indonesia

Article Info

Article history:
Submitted June 30, 2025
Accepted August 19, 2025
Published September 3, 2025

Keywords:
Electric vehicle;
BLDC motor;
energy efficiency;
geometry optimization;
PSO algorithm.

ABSTRACT

Gasoline vehicles (GVs) contribute significantly to global energy crises and environmental pollution, while electric vehicles (EVs) offer a more sustainable alternative. However, the current development and deployment of EVs are largely limited to ideal operating conditions, such as urban roads. To compete effectively with GVs, EVs must have drivetrain systems that maintain high efficiency even in non-ideal environments, including rural areas and rough terrains. This study proposes a geometry optimization method for a 1 kW Brushless DC (BLDC) motor to improve energy efficiency under three primary EV traction scenarios: climbing, acceleration, and cruising. The optimization targets nine geometric parameters—outer and inner stator radius, magnet thickness, rotor yoke thickness, shoe stator thickness, magnet width, shoe stator width, stator pole width, and back-iron thickness. The optimization is performed using a Particle Swarm Optimization (PSO) algorithm integrated with Finite Element Method Magnetics (FEMM) and analytical performance evaluation. The optimization constraints are derived from traction dynamics, weight, and volume limitations based on the regulations of the Indonesian Electric Vehicle Competition (Kompetisi Mobil Listrik Indonesia, KMLI). The results show that the optimized BLDC motor geometry can increase efficiency by up to 24.3% and torque by 11.3% compared to the baseline design. This research contributes a high-efficiency BLDC motor design tailored for dynamic EV traction demands under regulatory and extreme operational constraints, making it highly suitable for further development, including additional performance scenarios such as deceleration and cornering.

Corresponding Author:
Kurniawan,
Department of Electrical Engineering, Institut Teknologi Nasional Yogyakarta,
Babarsari Road, Caturtunggal, Depok, Sleman, Yogyakarta, 55281, Indonesia.
Email: *kurniawan@itny.ac.id

1. INTRODUCTION

The widespread use of gasoline vehicles (GVs) has resulted in two major problems: a fossil energy crisis and increased environmental pollution. As a more environmentally friendly alternative, electric vehicles (EVs) have attracted significant attention from industry, academia, and governments around the world due to their zero carbon emission characteristics [1][2]. In urban regions, EVs play a strategic role in reducing pollution levels, as transportation demands are generally higher compared to rural regions [1]. Additionally, higher income levels and better access to charging infrastructure make EV adoption more favorable in urban environments [3]. The relatively short travel distances in urban regions further enhance the suitability and attractiveness of EVs [1][4]. Urban settings offer ideal operating conditions for EVs, including short commuting distances, sufficient acceleration distance to reach optimal speeds, relatively flat road terrain, adequate power capacity in both the drivetrain system and energy source, and easily accessible charging infrastructure. However, to compete with GVs, EVs must also be capable of performing effectively under non-ideal conditions, such as those found in rural, agricultural, and mining environments.

In several EV competitions held across different countries, the performance evaluation scenarios closely reflected real operational challenges. These challenges were similar to those encountered by EVs in rural environments. In such settings, EVs had to operate under non-ideal conditions while also complying with strict

regulatory constraints. For example, the *Mileage Challenge* scenario in the international Shell Eco-Marathon (SEM) requires EVs to complete a race over a considerable distance within a limited time while minimizing electricity consumption [5]. The EV competition held at the Pike's Peak International Hill Climb featured a 12.42 mile course with an elevation ranging from 2.86 meters to 4.30 meters. The track with its 156 turns posed a significant challenge for EVs in terms of limited operating time per charge [6]. On the other hand, the *Kompetisi Mobil Listrik Indonesia* (KMLI), a national EV competition involving dozens of universities across Indonesia, features test scenarios that closely resemble rural EV usage. These performance tests include climbing, acceleration, deceleration, cornering, and cruising [7]. In this competition, most EV drivetrain systems utilize outer-rotor BLDC motors. The BLDC motor is a popular choice due to its structural simplicity, lightweight nature, broad operational speed range, low maintenance cost, and relatively high torque density and efficiency [8][9][10]. The outer-rotor configuration offers additional benefits, such as greater rotational inertia and the possibility of direct on-wheel installation, resulting in a more simplified mechanical system [11]. KMLI's regulations and test scenarios push EVs to operate at critical limits. Despite limited motor power capacity and restricted battery energy, both defined by competition rules, EVs are required to perform optimally across extreme operating conditions, particularly in climbing, acceleration, and cruising test scenarios. Each condition presents different traction requirements and motor rotational speed ranges, which significantly affect BLDC motor efficiency. At low rotational speeds and high traction loads, efficiency tends to be low due to dominant copper losses in the stator windings. Peak efficiency is achieved at a certain rotational speed range, but it drops sharply at higher rotational speeds due to increased iron core losses [11]. This is a crucial issue, as low efficiency leads to higher energy consumption, while the energy source is strictly limited. Consequently, energy efficiency becomes a key parameter in enhancing BLDC motor performance in EV applications. Recent advancements in BLDC motor technology have focused on geometry optimization to achieve maximum performance, as geometric improvements can significantly enhance efficiency [12]. Geometrical parameters such as slot size, stator pole width, magnet dimensions, rotor diameter, and stator diameter can be optimized to design high-efficiency BLDC motors [8][11][12].

Several recent studies have focused on improving the efficiency of BLDC motors as EV drivetrain systems through geometry optimization. Among them, Ozturk et al. [8] employed a genetic algorithm (GA) to optimize nine geometric parameters of a 1 kW outer-rotor BLDC motor, achieving an efficiency of 90.35%. However, this study prioritized torque density as the sole optimization constraint, without taking into account the overall traction requirements of the EV. Arifin et al. [12] conducted manual optimization on three geometric parameters of a 0.5 kW outer-rotor BLDC motor, namely slot depth, stator pole width, and Hallbach magnet configuration. This approach resulted in six geometry variants, with the highest efficiency reaching 94.27%. Unfortunately, the optimization method was carried out without considering any constraints. Budi et al. [9] focused on optimizing eight rotor geometry parameters of a 5 kW inner-rotor BLDC motor without including stator optimization. Performance evaluation was carried out using a FEMM-based numerical method and analytical approach, resulting in a maximum efficiency of 97.09%. However, this approach remained oriented toward motor–inverter compatibility rather than addressing the traction dynamics requirements of EVs. Hejra et al. [13] applied the Sequential Quadratic Programming (SQP) method to optimize nine geometric parameters of an outer-rotor BLDC motor. This study considered the motor's volumetric dimensions as optimization constraints and used Finite Element Analysis (FEA) to evaluate torque and flux density. The highest efficiency achieved was 92.24%, but the approach still did not take into account variations in traction load and motor rotational speed. Sundaram et al. [14] discussed the design formulation of a 2 kW high-torque BLDC motor using a selection method involving four combinations of stator slots and magnet poles with predefined geometric parameters. Each combination was analyzed using FEA, taking into account volumetric constraints (motor diameter and effective axial length), a rated torque of 50 Nm at a rotational speed of 400 rpm, and an EV range of 108 km per charge at a speed of 54 km/h. The highest efficiency, 90%, was achieved with an optimal BLDC motor design featuring 51 stator slots and 46 magnet poles. From these studies, it can be concluded that the majority of research has not yet considered the traction dynamics requirements of EVs to fully address the problem highlighted in our study—namely, that EVs must maintain high performance under varying and non-ideal operating conditions, such as those found in rural environments or during competitions. While the study conducted by [14] did account for harsh environments, non-ideal operation, and several strict constraints, the optimization approach remained manual and limited to only four design combinations. Therefore, our study is proposed to fill the identified research gaps.

The objective of our study is to develop a 1 kW outer-rotor BLDC motor geometry design that achieves balanced efficiency under climbing, acceleration, and cruising conditions, based on the test scenarios of the KMLI. These three scenarios represent typical traction dynamics requirements encountered when EVs are driven in rural regions or other non-ideal terrains. Nine geometric parameters of the BLDC motor—including outer stator radius, inner stator radius, magnet thickness, rotor yoke thickness, shoe stator thickness, magnet width, shoe stator width, stator pole width, and back-iron thickness—are optimized using the Particle Swarm Optimization (PSO) algorithm. This optimization is integrated with FEMM-based numerical methods and

analytical evaluations to assess the performance of the motor geometry. The optimization constraints are formulated through traction dynamics requirement analysis, weight requirement analysis, and volumetric requirement analysis, ensuring the resulting geometry meets the necessary specifications and performance requirements without violating KMLI regulations. Our study aids in the advancement of EV drivetrain systems designed to function effectively in non-ideal road conditions. These systems will also be capable of operating with limited powertrain capacity and energy availability, particularly in rural, agricultural, mining, or other harsh environments. This development is guided by regulations and test scenarios based on competition.

2. RESEARCH METHODS

This study employed a simulation-based approach to develop a BLDC motor geometry design that achieves efficiency balance across various EV traction requirements, specifically tailored for competition requirements in KMLI, by optimizing nine geometric parameters. The optimization is carried out using the PSO algorithm, with regulatory-based optimization constraints integrated with FEMM-based numerical methods and analytical approaches. The instrumentation and equipment specifications used in this study included FEMM 4.2 software for magnetic field simulation and flux distribution calculation of the BLDC motor. MATLAB R2015b was used for implementing the PSO algorithm, conducting numerical analysis, and visualizing data. Additionally, the study utilized hardware in the form of a computer equipped with an AMD A4-9125 RADEON R3 2.3 GHz processor and 8 GB of RAM. The research methodology is conducted systematically, as illustrated in Figure 1.

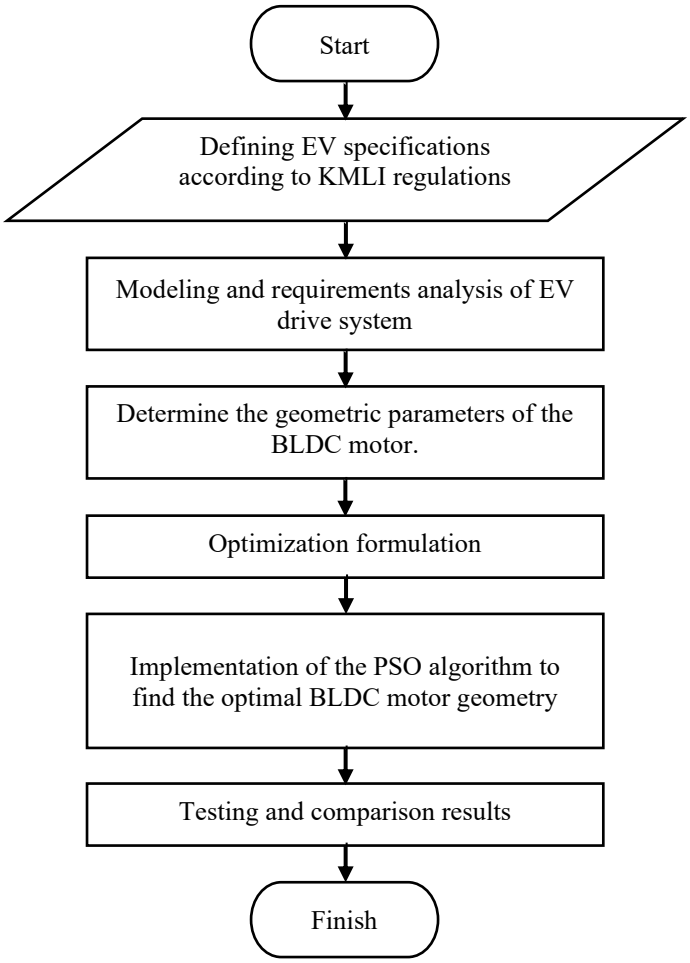

Figure 1. Research methods flowchart

2.1 EV Drivetrain System Modeling and Requirement Analysis

Modeling and requirements analysis is the initial stage in designing and determining the specifications of an EV drivetrain system to ensure its performance meets the desired criteria. The targeted performance criterion is an EV drivetrain system that maintains balanced efficiency across the three EV performance test scenarios without violating the regulatory limits set by KMLI. Therefore, the analysis of EV drivetrain requirements must be carried out based on the regulations and performance test scenarios defined in KMLI. The regulations set by the KMLI organizers are summarized in the EV specification data presented in Table 1.

Table 1. EV specification regulations

Symbol	Description	Value
$P_{nom_{drive}}$	Nominal power of the drivetrain system	$\leq 2 \times 1$ kW
E_{bat}	Battery capacity	≤ 2.2 kWh
$V_{nom_{bat}}$	Battery nominal voltage	≤ 48 V
$I_{lim_{BMS}}$	BMS current limit	100 A
m	Vehicle mass + driver mass	$180 + 50$ kg
r_{wheel}	Wheel radius	0.178 m
A_f	Frontal area	1.24 m^2
c_d	Drag coefficient	0.25
c_r	Rolling coefficient	0.01

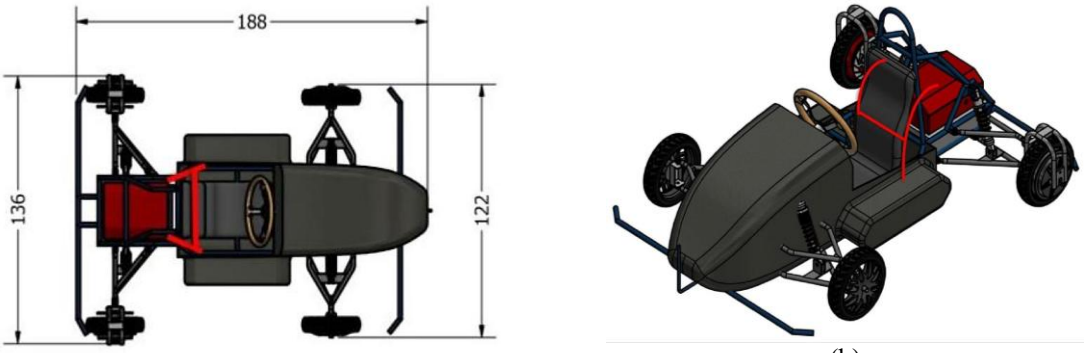

(a) (b)

Figure 2. (a) EV design top view, (b) EV design front-side view

Based on Table 1, the EV specification data represent parameters that directly influence the analysis of EV drivetrain requirements. The design and dimensions of the EV, which have been adjusted in accordance with KMLI regulations, are illustrated in Figure 2. The test scenarios used to evaluate EV performance in KMLI are presented in Table 2, while the other two test scenarios, namely deceleration and cornering are not discussed in this study, as they do not have a significant impact on the analysis of EV drivetrain requirements.

Table 2. EV performance test scenarios

Symbol	Description	Climbing	Acceleration	Cruising
φ	Track elevation angle	15^0	0^0	0^0
s	Track length	9.27 m	30 m	(5×700) m
ρ	Air density	1.225 kg/m^3	1.225 kg/m^3	1.225 kg/m^3
g	Gravitational acceleration	9.81 m/s^2	9.81 m/s^2	9.81 m/s^2
t	Traveling time	4.84 s	6.64 s	377 s
v_{start}	Start velocity	0 m/s	0 m/s	0 m/s

2.1.1 Traction Dynamics Requirement Analysis of the EV

The traction dynamics requirement analysis of the EV is carried out to determine the traction power required to overcome its resistive forces, as well as the minimum rotational speed and torque that must be generated by the EV drivetrain system under the three performance test scenarios described in Table 2. The traction dynamics requirement analysis is conducted using Equations (1) to (10).

$$v_{avg}(n) = mean\left(v_{start}(n), v_{end}(n)\right) \quad (1)$$

$$F_{aero}(n) = \frac{1}{2} \cdot \rho \cdot A_f \cdot c_d \cdot v_{avg}^2(n) \quad (2)$$

$$F_{roll}(n) = c_r \cdot m \cdot g \cdot \cos\left(\varphi(n)\right) \quad (3)$$

$$F_{grav}(n) = m \cdot g \cdot \sin\left(\varphi(n)\right) \quad (4)$$

$$F_{res}(n) = F_{aero}(n) + F_{roll}(n) + F_{grav}(n) \quad (5)$$

$$E_{kine}(n) = \frac{1}{2} \cdot m \cdot v_{end}^2(n) \quad (6)$$

$$E_{trac}(n) = \frac{\left(F_{res}(n) \cdot s(n)\right) + E_{kine}(n)}{3600} \quad (7)$$

$$P_{trac}(n) = \frac{E_{trac}(n)}{t(n)/3600} \quad (8)$$

$$\omega_{des}(n) = \frac{v_{avg}(n)}{r_{wheel}} \quad (9)$$

$$T_{des}(n) = \frac{P_{trac}(n)}{\omega_{des}(n)} \quad (10)$$

$$n = \{climbing, acceleration, cruising\}$$

In all n test scenarios, the EV starts from rest at an initial velocity v_{start}, where, according to Newton's Second Law, the EV undergoes acceleration, resulting in a final velocity v_{end} and an average velocity v_{avg}. F_{res} is the total resistive force acting on the EV, which is the sum of aerodynamic drag F_{aero}, rolling resistance F_{roll}, and gravitational resistance F_{grav}. Gravitational resistance only applies to routes with an elevation angle greater than 0°, specifically in the climbing test scenario. E_{kine} represents the kinetic energy required by the EV to overcome acceleration and inertial forces, while E_{trac} and P_{trac} are the traction energy and power needed to overcome total resistance. Specifically, in the climbing test scenario, even though the EV starts from rest, it does not accelerate significantly, as it tends to move at a constant velocity due to the climbing traction load. Therefore, the effects of acceleration and inertia can be neglected, and the traction energy required for climbing in Equation (7) can be rewritten as shown in Equation (11).

$$E_{trac}(climb) = \frac{F_{res}(climb) \cdot s(climb)}{3600} \quad (11)$$

Furthermore, in the cruising test scenario, the EV undergoes acceleration only over the first 30 meters, which accounts for 5.8% of the total cruising track length. As a result, the kinetic energy required to overcome acceleration and inertial resistance is only needed along this initial segment. For the remaining 94.2% of the track, the EV only contends with aerodynamic drag and rolling resistance. Therefore, in the cruising test scenario, the average velocity of the EV in Equation (1) can be rewritten as shown in Equation (12) to (14).

$$s(cruise) = s(cruise) - s(accel) \quad (12)$$

$$t(cruise) = t(cruise) - t(accel) \quad (13)$$

$$v_{avg}(cruise) = \frac{s(cruise)}{t(cruise)} \quad (14)$$

Based on the traction dynamics requirement analysis described above, three variations of the minimum required rotational speed ω_{des} and three variations of the minimum required torque T_{des} were obtained, which must be generated by the BLDC motor as the EV's drivetrain system for each test scenario. These three variations represent the operational range of the BLDC motor. The BLDC motor must have a rated rotational speed ω_{rated} that is higher than its operational rotational speed range to ensure that it operates within a safe and efficient rotational speed range [15], as estimated using Equations (15) and (19).

$$\omega_{rated} \geq \max\left(\omega_{des}(n)\right) \quad (15)$$

$$\omega_{rated} = \frac{V_{ph} - \left(I_{ph_{rated}} \cdot R_{ph}\right)}{ke} \quad (16)$$

$$I_{ph_{rated}} = \frac{P_{nom_{mot}}}{V_{nom_{bat}} \cdot \sqrt{3}} \quad (17)$$

$$P_{nom_{mot}} = \frac{P_{nom_{drive}}}{k} \quad (18)$$

$$ke = kt \quad (19)$$

In a three-phase star-connected motor, V_{ph} is the phase voltage, which is equal to the nominal battery voltage $V_{nom_{bat}}$ divided by the square root of three. The variable k represents the number of BLDC motors used in the EV drivetrain system, so $P_{nom_{mot}}$ denotes the nominal power for each BLDC motor. In a three-phase star connection, the rated phase current $I_{ph_{rated}}$ is equal to the rated line current, which is achieved at the rated rotational speed. R_{ph} is the phase winding resistance, which is influenced by the winding configuration, wire cross-sectional area, and stator slot size. The back-EMF constant ke is equivalent to the torque constant kt.

Furthermore, the BLDC motor must also generate an average torque T_{avg} that exceeds the average operational torque requirements to ensure it can withstand traction loads under the three test scenarios, as estimated using Equations (20) and (23).

$$T_{avg} \geq \frac{mean\left(T_{des}(n)\right)}{k} \tag{20}$$

$$T_{avg} = mean\left(T(n)\right) \tag{21}$$

$$T(n) = I_{ph}(n) \cdot kt \tag{22}$$

$$kt = \frac{T_{rated}}{I_{ph_{rated}}} \tag{23}$$

The torque T_{rated} refers to the torque of the BLDC motor when it operates at its rated rotational speed, and it is influenced by the motor's geometry. Consequently, both kt and ke are characteristics of the BLDC motor that are influenced by its geometry. The torque T produced by the BLDC motor varies with the phase current I_{ph}, while the phase current also varies with the operational rotational speed, which can be calculated by substituting Equation (16), and is expressed as Equation (24) and (25).

$$I_{ph}(n) = \frac{V_{ph} - \left(ke \cdot \omega(n)\right)}{R_{ph}} \tag{24}$$

$$E(n) = ke \cdot \omega(n) = V_{ph} - \left(I_{ph}(n) \cdot R_{ph}\right) \tag{25}$$

Based on Lenz's law, the back-EMF E is defined as the difference between the phase voltage and the voltage drop across the phase winding resistance. In this study, the three variations of the required rotational speed ω_{des} in the climbing, acceleration, and cruising test scenarios are used as reference parameters in the BLDC motor geometry optimization process. The goal is to develop a BLDC motor geometry that functions optimally and achieves high efficiency throughout the rotational speed range ω, which aligns with the variations of ω_{des}, as indicated in Equation (26). Moreover, ω_{des} serves as a reference parameter in the performance comparison stage. To evaluate the improvement of the optimized BLDC motor over the baseline motor, both must be tested under the same rotational speed range, ensuring a fair comparison, and calculated using Equation (26).

$$\omega(n) = \omega_{des}(n) \tag{26}$$

2.1.2 Weight Requirement Analysis of the EV Drivetrain System

The weight requirement analysis of the EV drivetrain system applies only to the rotating components, which directly influence inertial resistance during vehicle acceleration [16]. According to [17], the ideal total weight of the rotating drivetrain components, $m_{rot_{des}}$, should be 5% of the total weight of the EV, including the rider, and calculated using Equation (28). These rotating components include the permanent magnet, rotor yoke, wheel rim, and tire, whose weight is estimated using a numerical method based on FEMM and is defined as the rotor weight m_{rot} for a single BLDC motor. In this context, the weight of the permanent magnet and rotor yoke is highly dependent on the BLDC motor geometry produced by the PSO algorithm. The rotor weight must not exceed the ideal total weight of the rotating drivetrain components, which is calculated using Equation (27).

$$m_{rot} \leq m_{rot_{des}} \tag{27}$$

$$m_{rot_{des}} = \frac{0.05 \cdot m}{k} \tag{28}$$

2.1.3 Volumetric Requirement Analysis of the BLDC Motor

The volumetric requirement analysis aims to ensure that the size of the BLDC motor does not exceed the size of commercially available rims, specifically 10 inches in diameter with a tire thickness of 5.1 cm. The volumetric dimensions apply to each BLDC motor and include the motor diameter and the effective axial length. The designated motor diameter, $D_{mot_{des}}$, refers to the outermost diameter of the rotor, which must be smaller than the outer diameter of the wheel to allow sufficient space for mounting the rim and tire. Therefore, the motor diameter D_{mot} resulting from the PSO algorithm must not exceed the predefined limit $D_{mot_{des}}$, as defined in Equations (29) and (30).

$$D_{mot} \leq D_{mot_{des}} \tag{29}$$

$$D_{mot_{des}} = (2 \cdot r_{wheel}) - (2 \cdot tire_{thick}) - (2 \cdot velg_{thick}) \tag{30}$$

The variables r_{wheel}, $tire_{thick}$, and rim_{thick} denote the wheel's outer radius, tire thickness, and rim thickness, respectively. The effective axial length of the BLDC motor must be smaller than the total axial length of the EV drivetrain system, which must accommodate winding overhangs, bearing housing, and mechanical clearances on both sides of the motor [14]. The designated effective axial length of the BLDC motor, $L_{mot_{des}}$, is set as a constant value of 50 mm.

Based on the EV drivetrain system requirement analysis, four optimization constraints have been established and must be adhered to during the optimization process. These constraints are considered satisfied if all conditions specified in Equations (15), (20), (27), and (29) are met. The optimization constraints are intended to guide and ensure that the optimization process results in a BLDC motor geometry that meets the performance requirements for the three test scenarios without violating the regulatory limits set by KMLI.

2.2 BLDC Motor Geometry Parameterization

The BLDC motor studied in this research is a 1 kW outer-rotor type, which has nine geometric design parameters that need to be optimized. Table 3 presents these geometric parameters along with their lower and upper bounds.

Table 3. Optimized geometric parameters

Symbol	Description	Lower Bound (mm)	Upper Bound (mm)
r_{so}	Stator outer radius	80	90
r_{si}	Stator inner radius	50	60
t_m	Magnet thickness	3	9
t_y	Rotor yoke thickness	3	9
t_s	Stator shoe thickness	0.8	6.4
w_m	Magnet width	15.3	27.2
w_s	Stator shoe width	12.6	21.2
w_p	Stator pole width	3.9	9.4
t_b	Back-iron thickness	11.8	37.7

All geometric parameters of the BLDC motor are visualized in Figure 3. Additional geometric parameters that are defined as constants and not optimized are presented in Table 4. The stator winding used follows the common BLDC motor winding configuration typically employed in EV drivetrain systems, namely a three-phase star connection with a double-layer winding scheme [18][19][20].

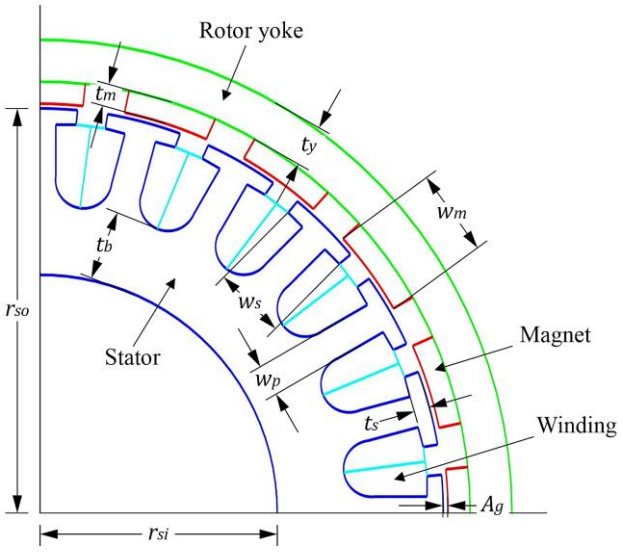

Figure 3. BLDC motor geometry

Table 4. Constant geometric parameters

Symbol	Description	Value
p	Number of magnetic pole pairs	10
n_s	Number of stator slots	24
D_{wire}	Wire diameter	2 mm
A_g	Air-gap	1 mm
L_{ax}	Effective axial length	50 mm
f_f	Fill factor	0.4
-	Magnet configuration	Radial

2.3 Optimization Formulation

The objective function is designed to achieve balanced efficiency for the BLDC motor across the three test scenarios. The efficiencies from the three scenarios are averaged to form a single objective function that must be maximized. The objective function is formulated as a fitness function, as expressed in Equation (31).

$$fitness = mean\left(\eta_{mot}(n)\right) \tag{31}$$

where η_{mot} represents the efficiency of the BLDC motor across three test scenarios, which is derived from a two-stage performance evaluation process. The first evaluation stage employed a numerical method based on FEMM to determine the magnetic field distribution, air-gap flux density, and rotor weight. The second stage employed an analytical method to compute the rated torque, T_{rated}, generated by the geometry of the BLDC motor, which was calculated using Equation (32) [10][20].

$$T_{rated} = N_{ph} \cdot I_{ph_{rated}} \cdot B_{g_{mean}} \cdot \frac{2 \cdot p \cdot p_{area}}{2 \cdot pi} \tag{32}$$

The variables N_{ph}, $B_{g_{mean}}$, p, and p_{area} represent the number of turns per phase, the average air-gap flux density, the number of pole pairs, and the area per magnetic pole, respectively. The torque generated by the BLDC motor originates from its electromagnetic torque [19]; thus, the output power P_{out} also corresponds to the electromagnetic power produced by the motor [9], which was obtained by substituting Equations (19), (22), and (25), resulting in Equation (33).

$$P_{out}(n) = E(n) \cdot I_{ph}(n) = \frac{ke \cdot \omega(n) \cdot T(n)}{kt} = \omega(n) \cdot T(n) \tag{33}$$

The output power of the BLDC motor is consistently lower than the power supplied by the battery because of total power losses, denoted as $P_{tot_{loss}}$. The efficiency and total power losses of the BLDC motor can be determined using Equation (34) and (36).

$$\eta_{mot}(n) = \frac{P_{out}(n)}{P_{in}(n)} \cdot 100\% \tag{34}$$

$$P_{in}(n) = P_{out}(n) + P_{tot_{loss}}(n) \tag{35}$$

$$P_{tot_{loss}} = P_{cu_{loss}} + P_{iron_{loss}} + P_{bearing_{loss}} + P_{Ag_{loss}} + P_{leak_{loss}} \tag{36}$$

The terms $P_{cu_{loss}}$, $P_{iron_{loss}}$, $P_{bearing_{loss}}$, $P_{Ag_{loss}}$, and $P_{leak_{loss}}$ refer to various types of power losses: copper losses, iron core losses, bearing friction losses, air-gap losses, and flux leakage losses, all occurring in the stator slots and windings, respectively. A comprehensive assessment of the total power losses is available in the analytical method conducted by [9].

2.4 Implementation of the PSO Algorithm

The PSO algorithm is an optimization method that imitates the collective behavior of organisms as they search for food in a specific environment. It is utilized to identify the most optimal parameters. It was first introduced by Kennedy and Eberhart [21]. In this study, the PSO algorithm is employed to identify the optimal configuration of the geometry parameters for the BLDC motor. The flow of the optimization process using the PSO algorithm is depicted in Figure 4. The swarm consists of 10 particles with initial positions initialized randomly, where each particle's position represents a combination of nine BLDC motor geometric parameters.

The BLDC motor geometry of each particle is evaluated numerically and analytically to determine its fitness value. In Figure 4, p_{best} refers to the best motor geometry parameters ever found by each particle individually, while g_{best} refers to the best geometry parameters found globally by the entire particle swarm during the optimization process. The optimization is performed iteratively. The iteration continues until a stopping criterion is met, which occurs when the current number of iterations reaches the predetermined maximum number. The hyper-parameters used in the PSO algorithm are presented in Table 5.

Table 5. Hyper-parameters of the PSO algorithm

Symbol	Description	Value
w	Weight inertia	0.75
c_1	Cognitive coefficient	1.8
c_2	Social coefficient	1.2
n_p	Number of particle	10
n_i	Number of maximum iteration	100

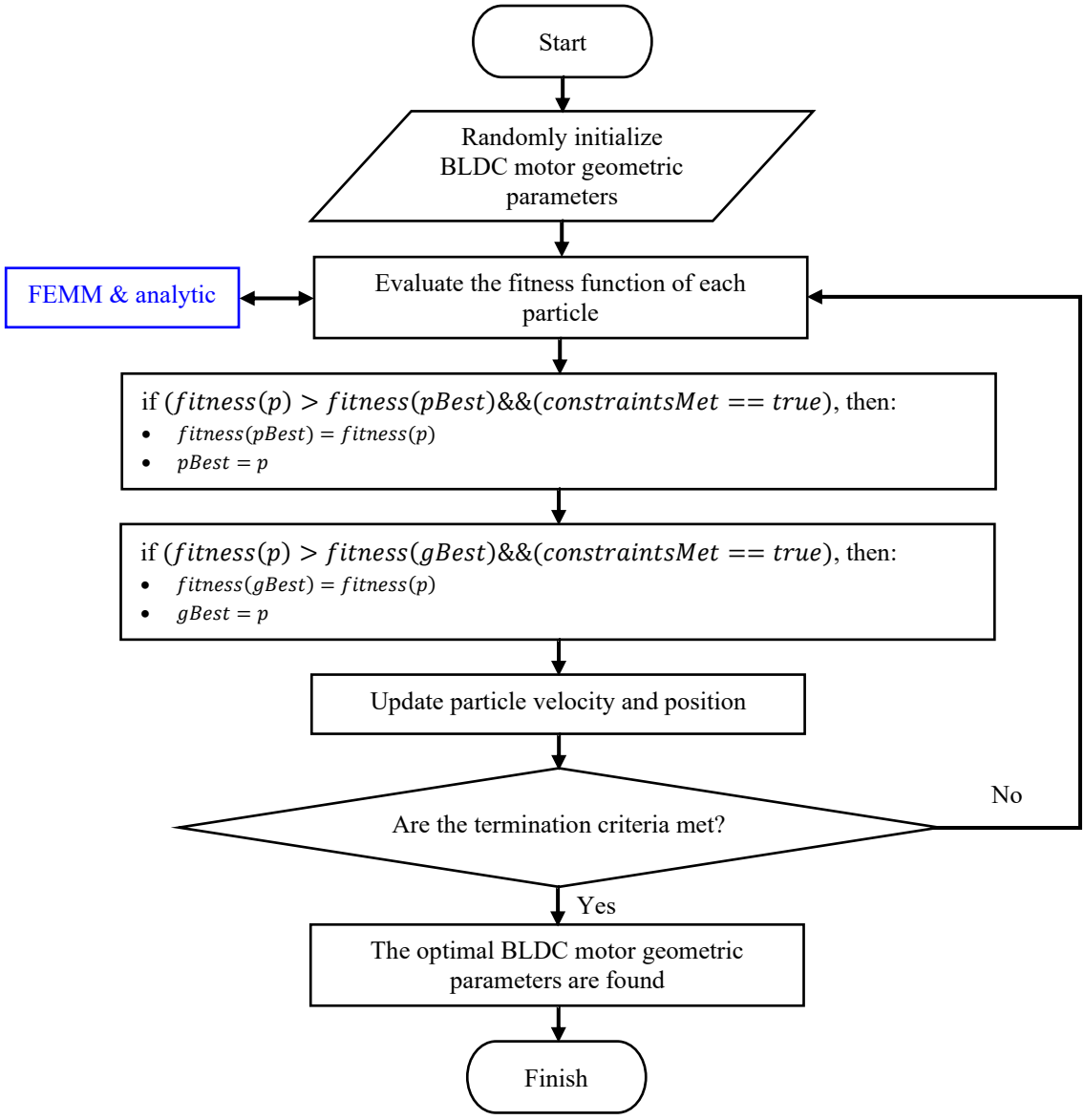

Figure 4. PSO algorithm flowchart

2.5 Validation of the EV Drivetrain Model

Validation was conducted to ensure that the modeling and simulation accurately represent the drivetrain system of the EV under study. The validation process consisted of comparing the simulated energy consumption per lap of the EV with actual field test results obtained under cruising conditions. The BLDC motor geometry was modeled using FEMM and integrated with an analytical approach to calculate the EV's energy consumption per lap using Equation (37).

$$E_{consumption} = P_{in} \cdot t \tag{37}$$

The EV's energy consumption per lap was measured in real field tests using a watt-hour meter. Both simulation and field testing were carried out under identical parameters and operating conditions as presented in

Table 1 and Table 2. The EV cruising test took place on a flat track, covering five laps. Each lap measured 700 meters, and the average lap time t was 75.4 seconds. The comparison between simulation and field test results is illustrated in Figure 5.

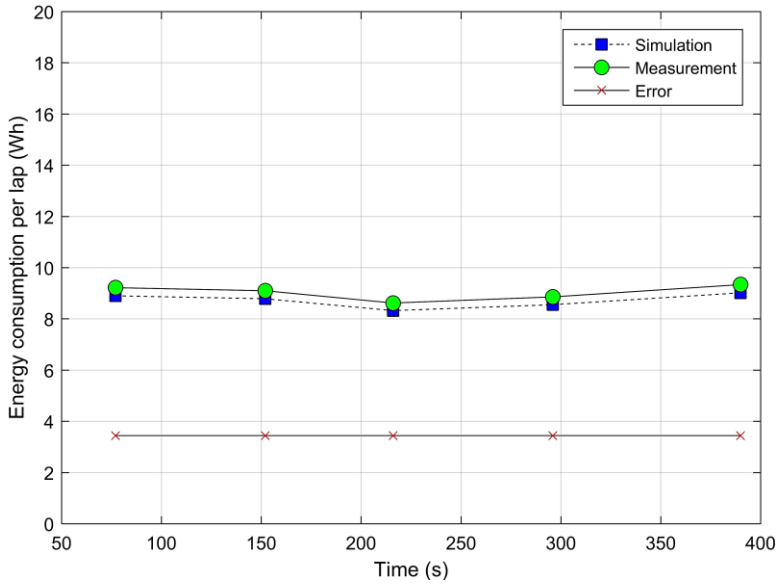

Figure 5. Simulation versus measurement of EV energy consumption per lap

Based on the comparison between the simulation and the field test results, an average error of 3.44% was observed. This value suggests that the simulation model effectively represented the system's behavior under the specified conditions and is thus considered suitable for implementation in this study.

2.6 Result Comparison Method

The result comparison method is conducted by comparing two performance parameters, namely torque and efficiency, under three performance testing scenarios between the optimal BLDC motor geometry and the baseline BLDC motor geometry. The baseline BLDC motor geometry is based on the design presented in a prior study by Sundaram et al. [14]. This geometry was selected for comparison because it applied constraints similar to those used in our study. Both motor geometries were tested and evaluated according to the KMLI regulations and performance testing scenarios under identical conditions (apple-to-apple comparison), specifically at the same rotational speed ranges and traction loads. This comparison was carried out to validate the performance improvement and novelty of the results obtained in our study.

3. RESULTS AND DISCUSSION

3.1 Results of the Optimized BLDC Motor Geometry

The fitness graph visualization of the PSO algorithm in Figure 6 demonstrates the evolutionary process of the BLDC motor geometry across multiple iterations. It starts with a low-efficiency geometry and progresses toward an optimal high-efficiency geometry, which is reached by the 100th iteration. The efficiency variance among the three test scenarios gradually decreased, indicating that a balance in efficiency was achieved across various EV traction requirements. The optimal rotor geometry features 20 NdFeB 37 MGOe permanent magnet bars arranged in a radial configuration, creating 10 pairs of magnetic poles. The optimal magnet thickness and pole area are nearly at the specified upper limit. In this scenario, the PSO algorithm favors the formation of thick and wide magnets to produce a larger and more uniform magnetic flux in the air gap. This design method assists in preventing demagnetization and promotes the generation of higher torque.

The optimal rotor yoke thickness is 7.870 mm, which is relatively thick but does not reach the upper bound. A rotor yoke that is too thin cannot effectively channel the magnetic flux between poles, leading to magnetic field distortion and torque degradation, while an excessively thick yoke increases rotor mass. The rotor yoke weight dominates the overall rotor mass, with the remaining mass contributed by the magnets. An overly heavy rotor results in higher mechanical losses and greater inertial resistance. The rotor yoke uses 1018 low-carbon steel, which is not overly sensitive to magnetic fields and is structurally strong. The optimal outer diameter of the rotor is determined by the outer stator diameter, the air gap, the magnet thickness, and the rotor yoke thickness and must remain smaller than the outer wheel diameter to allow space for the wheel rim and tire. The total axial length of the drivetrain system is 95 mm. The effective axial length of the BLDC motor is set to 50 mm, taking into account the stator winding overhang, bearing housing, and mechanical clearance on both sides.

The stator, which serves as the core for the windings, utilizes M-19 steel, a ferromagnetic material known for its low power losses. The optimization of the stator slot geometry relies on assessing stator winding resistance. A wider stator slot permits additional turns but also leads to increased winding resistance. The design of the stator slot geometry focuses on minimizing winding resistance, which in turn reduces copper losses, especially at low rotational speeds when the system is under traction loads. This optimization involves limiting the number of turns while still ensuring the generation of sufficient electromagnetic torque to effectively overcome the traction load.

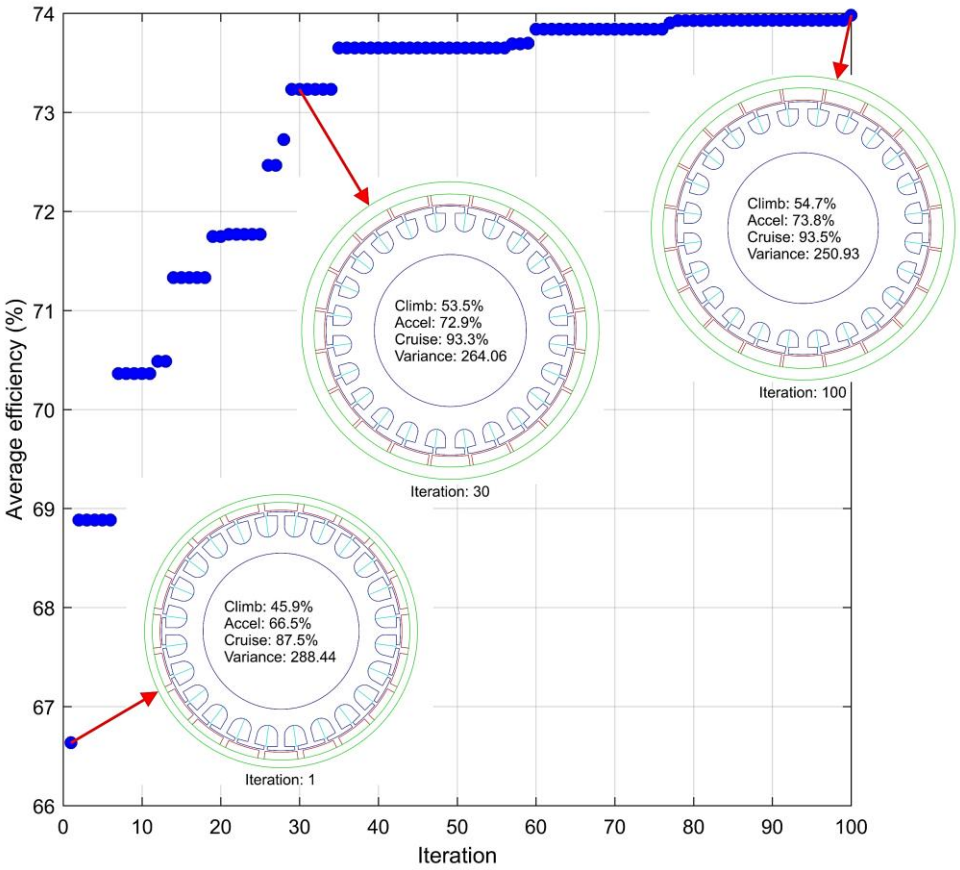

Figure 6. BLDC motor geometry evolution

The stator shoe's optimized geometry uniformly captured magnetic flux within the air gap, achieving 0.998 T average density. A larger stator shoe surface area facing the magnets results in smoother electromagnetic torque but may narrow the slot opening and complicate the winding process. An overly wide slot opening may increase flux leakage in the stator. On the other hand, to generate high electromagnetic torque, the stator shoe thickness must be increased, but excessive thickness may lead to higher eddy current losses. In addition to the stator shoe geometry, electromagnetic torque can also be increased by increasing the back-iron thickness. However, excessive back-iron thickness adds more weight to the stator. The optimized BLDC motor geometry parameters obtained through the PSO algorithm are presented in Table 6.

Table 6. Optimal BLDC motor geometric parameters

Symbol	Description	Optimal Parameters (mm)
r_{so}	Stator outer radius	85.190
r_{si}	Stator inner radius	50.767
t_m	Magnet thickness	8.307
t_y	Rotor yoke thickness	7.870
t_s	Stator shoe thickness	4.374
w_m	Magnet width	25.399
w_s	Stator shoe width	20.072
w_p	Stator pole width	6.526
t_b	Back-iron thickness	25.524

The stator winding configuration shown in Figure 7 employed a three-phase star connection with a double-layer winding scheme. The number of turns per stator slot is 16; the per-phase resistance is 0.034 Ω, which is influenced by the cross-sectional area of the copper wire, the fill factor, and the stator slot geometry.

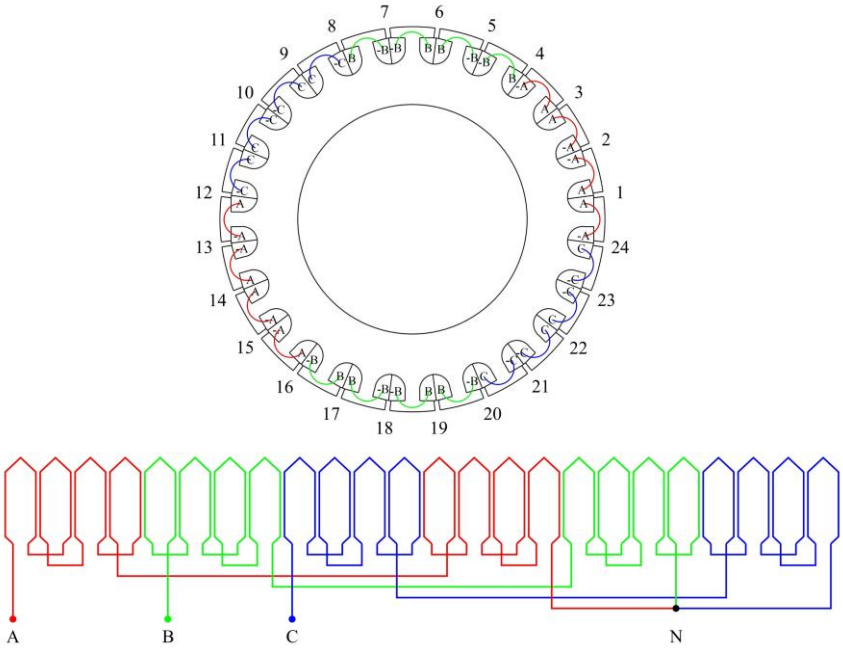

Figure 7. Stator winding configuration

3.2 Performance of the Optimal BLDC Motor Geometry

The performance of the optimal BLDC motor geometry is assessed by analyzing the distribution of the magnetic field and its effect on efficiency. The magnetic field distribution is estimated using a numerical method based on FEMM, as shown in Figure 8.

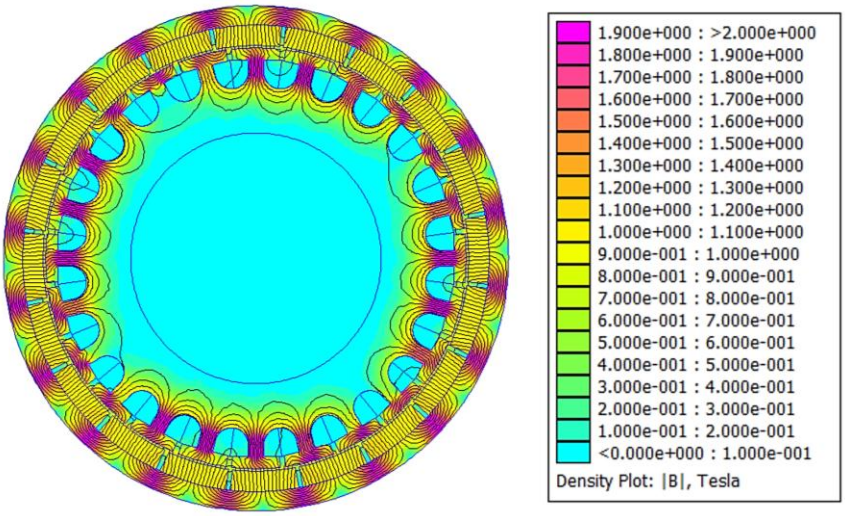

Figure 8. Distribution of magnetic fields

The magnetic flux generated by the permanent magnet field is distributed through the air gap and captured by the stator shoe. A wider stator shoe geometry allows for greater magnetic flux capture. The stator shoe captures the dispersed magnetic flux within the air gap, exhibiting higher flux density when oriented directly toward the magnetic poles. This configuration allows for a maximum air-gap flux density of 1.192 T. The root geometry of the stator poles features a curved profile designed to follow the natural path of magnetic flux. This design enables the flux to flow smoothly through each stator pole and back-iron, creating a laminar pattern that aligns with the curvature of the stator pole roots. The performance of the optimal BLDC motor geometry is evaluated based on its efficiency at different operational rotational speeds. According to the three test scenarios used in KMLI, there are three variations of operational rotational speed, each corresponding to different motor

efficiencies distributed along the efficiency curve. The efficiency curve with respect to variations in operational rotational speed is illustrated in Figure 9.

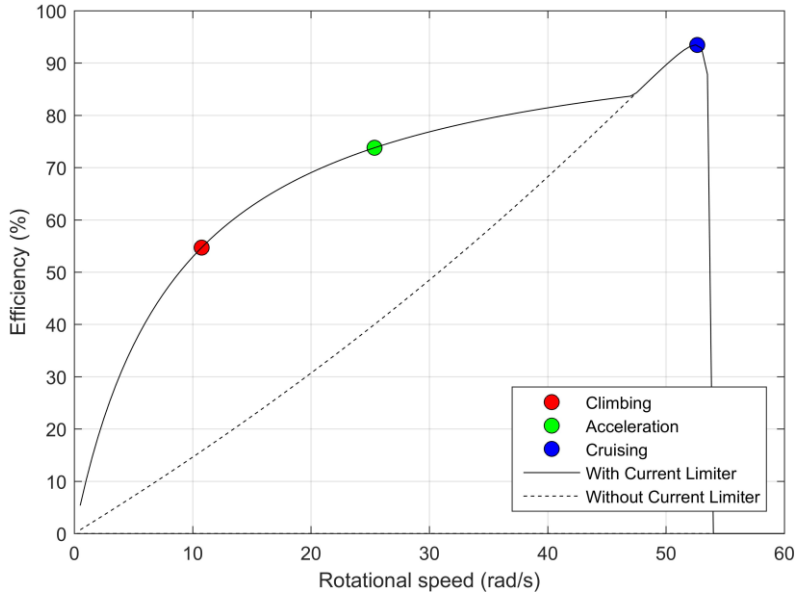

Figure 9. Optimal efficiency curve against operational rotational speed variations

In the climbing test scenario, the BLDC motor operates at a low rotational speed because of the high traction load, which results in an efficiency of only 54.7%. Operating at low rotational speeds under a heavy traction load results in considerable losses in the stator winding. In the acceleration test scenario, the BLDC motor operates at a moderate rotational speed due to acceleration and inertia loads, achieving an efficiency of 73.8%. In this situation, the motor fails to achieve its optimal rotational speed because the EV has not completely overcome the resistance from acceleration and inertia, which is attributed to the very short test distance of just 30 meters. As a result, the motor efficiency remains relatively low since the rotational speed is still far from its rated value. The maximum efficiency of 93.5% is achieved when the motor operates at 52.64 rad/s, which is very close to its rated rotational speed, as observed in the cruising test scenario.

The PSO algorithm aims to develop and position the optimal efficiency curve to align with the operational rotational speed range required by the EV drivetrain system for each test scenario. This is accomplished by optimizing the geometry of the BLDC motor to enhance efficiency within that defined range. In addition, the optimization constraints ensure that the three variations of operational rotational speed remain within the rated rotational speed range so that the BLDC motor operates at a safe and efficient speed. The PSO algorithm's effort to shift the efficiency peak toward the cruising speed point is an appropriate solution, as the cruising test scenario requires the EV to travel a relatively long distance, where high efficiency is critical. Higher efficiency implies lower energy consumption, which can extend the EV's driving range on a single battery charge.

Through the analysis of the curve in Figure 9, the significance of the difference between the theoretical and practical curves can also be observed. In the practical curve, the Battery Management System (BMS) imposes a phase current limitation of 100 A, which results in increased efficiency. This is particularly evident at low and medium rotational speeds when the BLDC motor experiences climbing and accelerating traction loads. The phase current limitation not only prevents overcurrent during excessive load conditions but also aims to minimize copper losses in the stator windings. Since copper losses are a quadratic function of the phase current, limiting the phase current to a constant value allows for a quadratic improvement in the efficiency of the BLDC motor as rotational speed varies.

3.3 Comparison of Results with Previous Studies

The performance of the optimal BLDC motor geometry and the baseline BLDC motor geometry was tested and evaluated under the same regulations and test scenarios described in Section 2.5. In Table 7, the BLDC motor geometry proposed by Sundaram [14] was tested under the KMLI regulations and test scenarios, with a power supply capacity limit of 1.1 kW per motor. In the climbing test, the efficiency was relatively low and slightly higher in the acceleration test. Generally, the efficiency increased with the rise in rotational speed due to copper losses. However, at rotational speeds higher than the rated speed, the efficiency significantly decreased again due to iron core losses. Both copper and iron core losses are quadratic functions of the rotational speed.

The efficiency curve, which is presented in Figure 10, demonstrates that the peak efficiency of Sundaram's BLDC motor geometry was not achievable within the rotational speed range specified by the KMLI test scenarios. In the climbing and acceleration tests, Sundaram's BLDC motor exhibited higher efficiency than

the optimized BLDC motor in our study. However, in the cruising test, Sundaram's BLDC motor was forced to operate above its rated rotational speed, causing its efficiency to drop drastically. This situation arose because the Sundaram's BLDC motor geometry was specifically engineered to function optimally at a rated rotational speed of 41.9 rad/s, a rated torque of 50.1 Nm, and a rated power of 2 kW. During the KMLI test scenarios, the BLDC motor demonstrated lower efficiency because it was unable to reach its optimal rotational speed. This limitation was due to traction loads that exceeded the motor's design specifications. Figure 10 shows a performance comparison between the optimal BLDC motor geometry and Sundaram's BLDC motor geometry as the baseline.

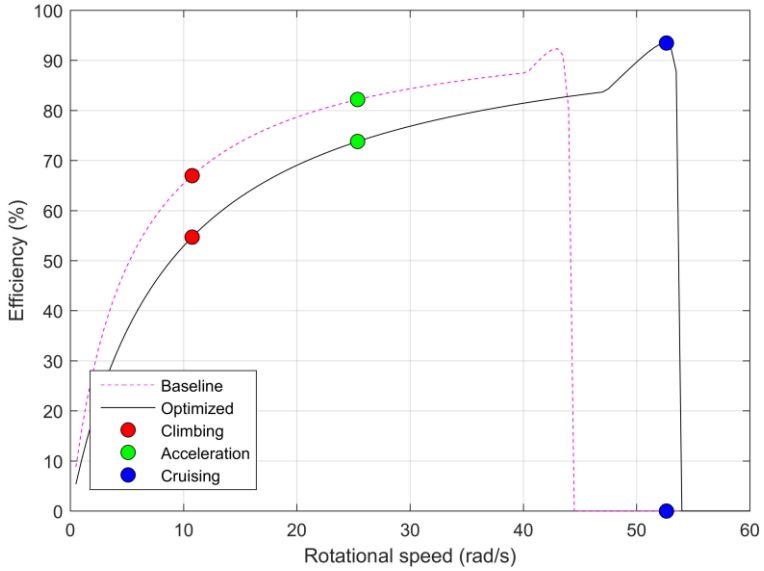

Figure 10. Baseline and optimized efficiency curve against operational rotational speed variations

The optimal BLDC motor geometry design presented in our study was specifically developed based on constraints identified during the analysis of drivetrain system requirements in accordance with KMLI regulations and the test scenarios used in the optimization process. When tested under the three performance scenarios, the optimized BLDC motor exhibited enhanced efficiency, showing an improvement of 24.3% compared to the baseline BLDC motor geometry. Additionally, the torque generated during the climbing, acceleration, and cruising tests was also higher, with an increase of 11.3%. These results indicate that the optimized BLDC motor geometry is capable of handling varying traction loads effectively across the three test scenarios. Table 7 provides a comparison of torque and efficiency between the optimal and baseline BLDC motor geometries, evaluated across the three KMLI test scenarios.

Table 7. Performance comparison between optimal and baseline BLDC motor geometry

Test scenarios	Rotational speed (rad/s)	Sundaram *et al.* (baseline)		Our study	
		Efficiency (%)	Torque (Nm)	Efficiency (%)	Torque (Nm)
Climbing	10.76	67.0	50.1	54.7	51.3
Acceleration	25.37	82.2	50.1	73.8	51.3
Cruising	52.64	0.0	0.0	93.5	10.4

4. CONCLUSION

The geometry of the BLDC motor, optimized through the PSO algorithm, demonstrates a significant improvement in performance when compared to the baseline geometry of the BLDC motor. This improvement is particularly evident in the magnetic flux distribution, which has a direct impact on both torque and efficiency. A more uniform flux distribution is achieved through a wide stator shoe design and curved stator pole roots, allowing the magnetic flux to follow its natural path and resulting in an optimal peak flux density in the air-gap region. The optimized BLDC motor geometry produces an optimal air-gap flux density, leading to a torque increase of 11.3% compared to the baseline geometry. Furthermore, the optimized geometry shows an efficiency improvement of up to 24.3% across the three KMLI test scenarios (climbing, acceleration, and cruising), with the highest efficiency achieved during the cruising test scenario due to the alignment of the efficiency peak within the corresponding operational rotational speed range. The optimal efficiency variance of 250.93 across these test scenarios indicates that efficiency balance has been achieved for the three variations of EV traction requirements. The PSO algorithm's strategy of positioning the efficiency peak at the cruising speed range is a well-suited approach, considering that the cruising scenario requires the EV to travel over a relatively long distance, where

high efficiency is crucial. High efficiency contributes to reduced energy consumption, thereby extending the EV's travel range per battery charge. The study indicates that the phase current limitation implemented by the BMS enhances efficiency, particularly during climbing and acceleration tests. The main advantage of this 1 kW BLDC motor geometry optimization method lies in its ability to tailor the drivetrain system's performance to specific traction requirements based on the regulations and test scenarios of the KMLI, particularly for climbing, acceleration, and cruising. The optimization method was not restricted to BLDC motors with a power capacity of 1 kW; it was also relevant for BLDC motors with greater power capacities. However, a limitation of our study is that it does not yet address two additional test scenarios, deceleration and cornering. Future work should incorporate these two scenarios into the formulation of the optimization constraints and objective function, as deceleration and cornering are integral parts of real-world EV dynamics. These conditions can significantly impact the overall performance of the BLDC motor, including transient torque response, thermal stability, and efficiency under deceleration or lateral loading conditions.

REFERENCE

[1] Z. Yan, H. Ding, and L. Chen, "The analyzing the role of electric vehicles in urban logistics: A case of China," *Front. Environ. Sci.*, vol. 11, Art. no. 1128079, 2023. http://dx.doi.org/10.3389/fenvs.2023.1128079

[2] S. Ma, K. Chen, and Q. Zhang, "Analysis of multi-objective optimization design of interior double radial and tangential combined magnetic pole permanent magnet drive motor for electric vehicles," *World Electr. Veh. J.*, vol. 15, Art. no. 142, 2024. http://dx.doi.org/10.3390/wevj15040142

[3] R. Kumar, "Electric vehicle adoption in urban areas: socio-economic factors and policy implications," *Shodh Sagar Journal of Electric Vehicles*, vol. 1, no. 2, pp. 14–19, 2024. http://dx.doi.org/10.36676/jev.v1.i2.11

[4] J. Ma *et al*., "Analysis of urban electric vehicle adoption based on operating costs in urban transportation network," *Systems*, vol. 11, no. 3, Art. no. 149, 2023. http://dx.doi.org/10.3390/systems11030149

[5] Z. Pusztai, P. Kőrös, F. Szauter, and F. Friedler, "Implementation of optimized regenerative braking in energy efficient driving strategies," *Energies*, vol. 16, no. 6, Art. no. 2682, 2023. http://dx.doi.org/10.3390/en16062682

[6] E. Håkansson and B. Dubé, "Winning approach: selection criteria for competitive battery powered racing vehicles," *World Electr. Veh. J.*, vol. 8, no. 1, pp. 160–171, 2016. http://dx.doi.org/10.3390/wevj8010160.

[7] Marwansyah, Panduan Kompetisi Mobil Listrik Indonesia XIII – 2024 [Guide to the Indonesian Electric Car Competition XIII - 2024], Bandung, Indonesia: KMLI, 2024. [Online]. Available: https://kmli.polban.ac.id/panduan-kmli-xiii/. Accessed: Aug. 25, 2025. (in Indonesian)

[8] O. Tosun, K. Toker, O. Tosun, N. F. O. Serteller, and V. Topuz, "The design, optimization, and experimental study of hub and axial flux BLDC motor under operating conditions for light electric vehicles," *Adv. Sci. Technol. Eng. Syst. J.*, vol. 8, no. 3, pp. 272–282, 2023. http://dx.doi.org/10.25046/aj080330

[9] B. Azhari, P. Irasari, and P. Widianto, "Design and simulation of 5 kW BLDC motor with half-buried permanent magnets using an existing stator body," *Int. J. Power Electron. Drive Syst.*, vol. 12, no. 4, pp. 2030–2043, 2021. http://dx.doi.org/10.11591/ijpeds.v12.i4.pp2030-2043.

[10] C. Kumar, D. M. Mary, and T. Gunasekar, "MOCHIO: a novel multi-objective coronavirus herd immunity optimization algorithm for solving brushless direct current wheel motor design optimization problem," *Automatika*, vol. 63, no. 1, pp. 149–170, 2022. http://dx.doi.org/10.1080/00051144.2021.2014035

[11] A. Kerem, "Design, implementation and speed estimation of three-phase 2 kW out-runner permanent magnet BLDC motor for ultralight electric vehicles," *Electr. Eng.*, vol. 103, no. 5, pp. 2547–2559, 2021. http://dx.doi.org/10.1007/s00202-021-01279-5.

[12] Z. Arifin, I. W. Adiyasa, and M. A. H. Rasid, "Design optimization analysis on the performance of BLDC motors on electric bicycles," *J. Phys.: Conf. Ser.*, vol. 2406, Art. no. 012016, 2022. http://dx.doi.org/10.1088/1742-6596/2406/1/012016

[13] H. Msaddek, A. Mansouri, and H. Trabelsi, "Optimal design and cogging torque minimization of a permanent magnet motor for an electric vehicle," *Teh. Vjesn.*, vol. 30, no. 2, pp. 538–544, 2023. http://dx.doi.org/10.17559/TV-20220815140808.

[14] M. Sundaram *et al*., "Design and FEM analysis of high-torque power density permanent magnet synchronous motor (PMSM) for two-wheeler e-vehicle applications," *Int. Trans. Electr. Energy Syst.*, vol. 2022, Art. ID 1217250, 14 pp., 2022. http://dx.doi.org/10.1155/2022/1217250

[15] M. As-salaf and Syahrial, "Simulasi Pengaturan Kecepatan Motor BLDC menggunakan Software PSIM [*Simulation of BLDC Motor Speed Control using PSIM Software*]," *MIND J.*, vol. 6, no. 1, pp. 103–117, 2021. https://doi.org/10.26760/mindjournal.v6i1.103 (in Indonesian)

[16] S. Torabi, M. Bellone, and M. Wahde, "Energy minimization for an electric bus using a genetic algorithm," *Eur. Transp. Res. Rev.*, vol. 12, no. 1, p. 6, 2020. http://dx.doi.org/10.1186/s12544-019-0393-1

[17] K. N. Genikomsakis and G. Mitrentsis, "A computationally efficient simulation model for estimating energy consumption of electric vehicles in the context of route planning applications," *Transp. Res. D*, vol. 50, pp. 98–118, 2017. http://dx.doi.org/10.1016/j.trd.2016.10.014

[18] O. Ustun, G. Tanc, O. C. Kivanc, and G. Tosun, "In pursuit of proper BLDC motor design for electric bicycles," in *Proc. 2016 22nd Int. Conf. Electr. Mach. (ICEM)*, 2016, pp. 1808–1814. http://dx.doi.org/10.1109/ICELMACH.2016.7732769

[19] V. Bogdan, M. Adrian, L. Leonard, B. Alexandra, S. Alecsandru, and N. Ionut, "Design and optimization of a BLDC motor for small power vehicles," in *Proc. SIELMEN 2021—11th Int. Conf. Electromech. Energy Syst.*, 2021, pp. 438–443. http://dx.doi.org/10.1109/SIELMEN53755.2021.9600327.

[20] Y. Cheng, X. Lyu, and S. Mao, "Optimization design of brushless DC motor based on improved JAYA algorithm," *Sci. Rep.*, vol. 14, Art. no. 5427, 2024. http://dx.doi.org/10.1038/s41598-024-54582-z

[21] Y. U. Nugraha, A. Cahyadi, M. N. Yuniarto, and I. Sidharta, "Design optimization for torque density in brushless DC motor with IPM V-type using PSO method," *IOP Conf. Ser.: Mater. Sci. Eng.*, vol. 694, Art. no. 012009, 2019. http://dx.doi.org/10.1088/1757-899X/694/1/012009